Numerical Simulation of Compacting Process of a Multi-stepped Part - Comparison with Experiments -

P. Mosbah [1], S. Shima [2], A.M. Habraken [3] and R. Charlier [3]

[1]Mechanical Engineering Department, University of Wales Swansea, Swansea, SA2 8PP, United Kingdom [2]Department of Mechanical Engineering, Kyoto University, Sakyo-ku, Kyoto, 606-8501 [3]Département MSM –University de Liège, 6 Quai Banning, 4000 Liege, BELGIUM

SYNOPSIS

From experimental data for an iron powder and constitutive equations based on the modified Cam-Clay model, simulation of an axi-symmetric multi-stepped part has been achieved. In the first part of this paper, details of the constitutive relation are discussed. In the second part, the simulation of a compaction process for a multi-stepped part has been carried out. The phenomena arising along the compaction are thereby discussed. Notably, it has been shown that the piece surprisingly rises from the lower punch during the compression. It has also been shown that defects in the piece could occur at the end of the compression, which is partly confirmed by experiments. In the third part of this paper, results of numerical simulation are compared with experiments and it is shown that the forces exerted on the tools are in the same range that the experimental ones. Finally, the conclusion compiles all observations made during the study and shows some ways to improve the modelling.

keywords: compaction, multi-stepped part, simulation, tool kinematics, slip crack

1 INTRODUCTION

For many years, research on the modelling of the powder forming process has increased owing to the growing activity in this sector and the need for the metal powder manufacturers to rationalize the process. Numerical simulations are considered as a way to achieve this objective; knowing the final characteristics and dimensions of a part it would then be possible by numerical simulations to optimize the form and the kinematics of tools in order to avoid defects in the part after compression. This method would then be less costly than experiment to determine step by step the appropriate set of parameters that may require for designing new tools. Nevertheless, in order to achieve this "ideal" it is important to link numerical simulations and experiments to ensure that the numerical simulations are reliable. This was the objective of *the international research program on the mechanics of metal powder forming* [1)] whose results have been published in Ref. 2). For this program, some experimental measurements, such as the forces exerted on the tools and the variation of density throughout a compact after ejection, have been achieved respectively during and after the compacting some pieces. Hence, from these data, it is possible to compare the results of calculation with those of experiment.

In this paper, the implementation into the finite element code LAGAMINE[3)] of the proposed constitutive relation is first detailed and discussed. From the kinematics and geometry of a multi-stepped part described in Ref. 2), results of simulation are presented. From these results, phenomena arising during the compaction are discussed at each step of the compaction. This

allowed showing some events possibly generated inside the part by the particular kinematics of the lower inner punch. Results obtained are also compared with provided experimental results. The obtained differences are discussed and some explanations are given.

Before going into details of the results of simulation, we shall first present powder and its modeling and then geometry of the part concerned and kinematics of tools. More complete reference can be found in Refs. 4-7).

2 POWDER AND ITS MODELLING

2.1 Powder

The characteristics of the iron powder used as base for experiments were:
4% Nickel,
1.5% Copper,
0.5% Molybdenum,
Particle size range: 20 to 210 μm,
Lubricant: 0.5% graphite and 1% wax,
Apparent density: 3040 kg/m^3,
Density of the dense material: 7810 kg/m^3.

2.2 Constitutive relations for powder

The used constitutive relation is similar to the modified Cam-Clay[7]. This model is associated and can be represented as an ellipsoid as shown in Fig.1 passing through the origin in the deviatoric stress-mean stress plane, q-p. We treat compressive stress as positive. We have

$$p = \frac{\sigma_{ii}}{3}, \tag{1}$$

$$q = \sqrt{(3/2)\sigma'_{ij}\sigma'_{ij}} \tag{2}$$

and

$$\sigma'_{ij} = \sigma_{ij} - \delta_{ij} p . \tag{3}$$

The equation for the ellipsoid is written by

$$q^2 + M^2 p(p - p_0) = 0 \tag{4}$$

where

$$p_0 = p_a (\rho / \rho_a)^n \tag{5}$$

and M, Pa, ρ_a are material constants and ρ being the density of the material after unloading[8]. This ellipsoid has been fitted by linear regression on triaxial tests. The values, M, Pa, ρ_a found for the iron powder described above are as follows[1]:

M=1.47, Pa=0.12MPa, ρ_a=2430 Kg/m^3.

In conjunction with the plastic modelling the elastic proprieties of the powder, Young modulus and Poisson's ratio, were assumed to be constant as 150 MPa and 0.3, respectively. Although the elastic parameters are actually not constant during the compression, as shown in Refs. 8 and 9; this should not affect the results significantly because the elastic behaviour mainly arises during unloading which has not been simulated in this study.

Recently there have been a lot of discussions on the constitutive equations for powders. For instance, the flow rule may not be associated with the yield function[9]; the material becomes anisotropic during die compaction[11,12]; metal powders may be sensitive to the third stress invariant and this phenomenon may be important for modelling unloading and ejection stages during die compaction, i.e. when the radial stress is higher than the axial stress. For simplicity, these aspects of the material behaviour were neglected in this paper.

The constitutive relation presented above has been introduced into a general purpose finite element code, LAGAMINE, which has been developed at the University of Liège[3]. The integration technique used in this code has shown an efficiency in terms of performance and stability [6].

3 CASE STUDY CALCULATION

3.1 Shape of compact

Finite element analysis of a multi-stepped part shown in Fig.2[1] has been carried out. This part is axi-symmetric and looks like a pulley. The initial and final dimensions of the piece are listed in Table 1. The ratio of the final to the initial height is about 2. This implies that, in the absence of horizontal deformation, the ratio of the final to the initial average density is also 2 (see below). We shall call in this part the zones A, B and C as shown in the figure.

The initial density used for this simulation was 3470kg/m^3. This represents a relative density of about 0.47. Note that this density is proposed by Häggblad et al.[1], whereas Kergadallan et al.[2] suggest that the density could be different in the upper and the lower part (zones A and B in Fig.2). They proposed to divide the whole zone into two: the upper part with a higher density and the lower part with a lower (zone C). Such variation in density during the die filling has been studied experimentally by Boccini[16] and will be estimated in further calculation[17].

3.2 Description of kinematics

The compression of the part is decomposed into four stages (Figs. 3, 4 and Table 2). During all stages, the lower outer punch (tool 2) remains immobile, whereas the upper punch (tool 1) compresses the part continuously. Thus, the movement of tool 1 allows controlling the total height of the piece (h_2 in Fig. 2) whereas height h_1 is controlled by the displacement of the lower inner punch (tool 3 in Fig.3). The rate displacement of tool 3, as it can be seen in Fig.4, is not constant during the compression. This variation along the compression allows regulation of the behaviour of the piece around the inner corner and in the rim (the right side of the junction rim-hub). As an example, Kergadallan et al.[2] have shown that, for pieces with almost the same initial and final dimensions, defect may or may not occur in the piece, according to the kinematics of tool 3. Numerical simulations also confirm this observation[17]. In Table 4, the height ratio, h_1/h_2, at the end of each stage is also listed.

The displacement of the core rod and die (tools 4 in Fig.3) leads a decrease in the friction between the powder and the tools by reducing the relative displacement in between. However, for this simulation the friction coefficient of 0.08 as proposed by the international program[1] is quite small in comparison with the one usually measured[1,9,18] especially in the early stage of the compression. Therefore the movement of 4 should give a small influence on the global behaviour of the structure.

3.3 Calculations

The mesh used for the simulation is shown in Fig. 5. The mesh consists of 480 four-node solid elements with four integration points and 120 three-node contact elements with five integration points. The tools, punches and die are assumed as rigid and do not require to be meshed. More detail about using a rigid foundation can be found in Refs. 3) and 19). Note that during the simulation of the compression, the use of rigid foundation is realistic because the rigidity of the tools is very large in comparison with the powder. During the ejection step which we do not treat here, on the other hand, the rigidity of the tools may have an influence of the so-called spring back.

4 RESULTS AND DISCUSSION

4.1 Results of simulation

Figs. 6 through 9 show the calculated density distributions at the end of different steps of the simulation. The compression starts with a height h_{1init} which is about half of h_{2init} (see Fig. 2). During the compaction at the end of each stage, see Table 2.

During the first stage, the rate of displacement of the inner lower punch (tool 3) is nearly a half of that of the upper punch (tool 1). Because of the small friction coefficient, the mesh deforms almost horizontally (see Fig. 6). Note that the density would be completely uniform if the ratio of h_{1init} to h_{2init} and the ratio of the rate displacement of tool 1 to that of tool 2 were the same, and the friction coefficient were null. Because of the friction at powder-tool interfaces, density between top punch 1 and tool 3, in particular near the both corners of top punch, increases; density near tool 2 (bottom of zone C) also increases, while around the right-hand side of the junction (around upper part of zone C) the density is the lowest. These are due to that although tool 2 does not move, tool 3 moves downward.

During the second stage, the velocity of tool 3 is more than a half of that of top punch 1 (the ratio is 0.75), while the ratio h_1/h_2 is just above 0.5 at the start of stage 2, and tool 2 remains still. This means that when focusing on the compaction in zone C, tool 2 moves upward at a velocity of more than a half the velocity of top punch 1 in relation to tool 3, hence density in this zone increases and becomes higher than other zones. And at the same time, the rim compresses and the element of the left side of the corner is stretched and rises from the lower inner punch 3. As a result, the right and the left sides of the junction rim-hub deforms differently (see Fig. 7).

During stage 3, tool 4 does not move, but since friction is so small that on the whole the density increases but the distribution seems to be qualitatively similar to that in stage 2. However, since the ratio of the velocity of tool 3 to that of tool 1 in relation to the ratio h_1/h_2 is even larger than in stage 2, the tendency in density increase is similar to that in stage 2 or even enhanced. The density in zone C and neighbouring area in zone B thereby becomes higher than in other part of zone A. The rate of displacement of tool 3 remains unchanged whereas for tool 4 it becomes null. As specified before, the friction coefficient for this simulation is fairly low (0.08) and hence the movement of tool 4 (die and core rod) does not seem to give a great influence on the global behaviour of the structure.

The large displacement difference between the right and left sides of the junction rim-hub stretches the element at the left side of the junction. It comes in contact with the rim that is still compressed and the left side of the junction dilates. In Fig.8, it can be seen that the mesh

surrounding the corner is certainly not fine enough. This is especially visible for the left side of the inner corner. It seems also clear that the gradient of density in this element is too large and may require to be remeshed. The remeshing of the structure, in particular by adaptive remeshing, will be treated in further studies[19].

During the fourth stage, the displacement of tool 2 becomes null and the upper punch (tool 1) compresses all the structure. Due to immobility of tools 2 and 3, the height h_1 remains unchanged and the density increases mainly in the upper part (zones A and B). Consequently, in stage 4 the average density becomes higher in the upper part than in the lower (see Fig. 9). Further, it can be seen that a defect is predicted at the left side of the corner. This defect may have been observed as a consequence of the coarse mesh in this zone. However, as we have seen above, when we employ the kinematics shown in Fig.4 (Table 2), the density increase differs from zone to zone. Therefore, the defect observed in stage 2 onward can occur. This agrees with the experimental results by Kergadallan et al. [2] and is justified by the explanation by Takemoto[20]. This defect is due to: "an unsuitable compression kinematics". Takemoto[20] shows that such crack occurs when a thin portion in a compact with higher density penetrates into a portion with a lower one. This seems to be the case in our simulation. Thus, even if the mesh is not fine enough, it seems that it is possible by numerical simulation to predict the occurrence of such a defect. With a finer mesh, we would be able to obtain a more accurate result on its occurrence.

Since slip cracks are located along the lines on which both sides move in tangential direction at different speeds, the magnitude of the shear stress can be a good indicator of the occurrence of a crack, when the crack is not visible. The shear stress in the structure is shown in Fig. 10. As it can be seen, the shear stress around the "crack" is as high as 244 MPa. This is a high value and can be a sign of an initiation of crack. Such high values can be avoided by an appropriate kinematics.

4.2 Comparison with experiments

After describing phenomena arising possibly during the compaction, this section will focus on the experimental results, in particular on density after ejection and the force exerted on the tools. Hence, it will be possible to compare experimental and simulation results in order to ensure the reliability of the modeling procedure[2,6]. Although the density in the part has been measured after ejection whereas the simulated results are given at the end of the compaction (before unloading), this difference may be neglected considering that the sample is rigid enough. This is certainly the case if the behavior of the compact is elastic with a large bulk modulus. This is dubious when plastic strain occurs during both unloading and ejection.

The measured densities, reproduced from Ref. 2) and the calculated densities are shown in Table 3. The measured ones are given for zones 1 to 5 as shown in Fig.11. The measured density is nearly uniform and therefore is not very different from the average density, which can be found by the ratio:

$$\textit{final density /initial density=initial volume/final volume} \qquad (6)$$

Thus knowing the final and initial dimensions of the sample, it is easy to calculate the final density; this is 7070 kg/m^3 for this calculation. The average measured density is slightly lower than the one calculated by (6).

The density found by the calculation is higher than the experimental one in the upper part (zone A), especially when going to the centre of the sample. In the lower part (bottom of zone C) it is lower. These differences may be due to the use the simplified constitutive equation as expressed by Eqs. (4) and (5). They may also be explained by plastic dilatancy arising during both unloading and ejection phases as suggested by Kergadallan et al.[2)]

Table 4 and Fig.12 show respectively the measured forces at the end of the compression and the forces found by the simulation. In Fig.12 it can be seen that the three curves present some breaking points at the time where the kinematics change. The upper force increases almost continuously, changing the curvature at time 0.39s and 0.96s due to the change in the displacement rate of the inner lower punch: at 0.39s it increases passing from 12.14mm/s to 19.44mm/s and stops at 0.96s. Therefore, at time 0.39s, the force on the inner lower punch presents a plateau and again increases in the later stage; at 0.96s it increases more sharply because strain rate gets higher in the upper part (due to the immobility of the lower inner punch). The forces exerted on the lower outer punch present an additional breakpoint due to the stopping of the movement of the die at 0.82s. As it can be seen in Fig.12, this does not give a large influence on the force exerted on the others tools. As noticed before, this is due to the small friction coefficient.

Comparison with the experimental values at the end of the compaction shows that the upper force, lower inner force and lower outer forces are respectively 21%, 10% and 53% lower than the experimental ones. To explain these differences accurately would need further study but they may be due to the following.

According to some experimental results[1,7,19)], the present friction coefficient at powder-die interfaces seems too small. This gives an influence on the magnitude of the upper force and lower force. As an example, it is common that in the case of the compression of a simple cylindrical piece a bigger friction coefficient gives a higher upper force and lower bottom force. For the present piece, the behavior is more complicated because the particular motion of the lower inner punch, but if the friction coefficient was higher, we could intuitively assume that the forces on both the upper and lower outer punches could be higher. The constitutive relation used here may be attributed to the differences. The difference in the lower outer force seems to be larger than other forces, and it should be examined further. Thus, together with friction coefficient at the powder-tool interfaces and elastic properties of compact should further be studied.

In the present paper, we treated only one kinematics of tools. We should also investigate the effects of tool kinematics on density distribution and defect formation, so that we are able to give useful information for process design for producing compacts with complicated shapes.

5 CONCLUSIONS

In this paper, a numerical simulation of a real part has been presented. In the first part, the phenomena arising inside the piece have been described. These data are difficult or sometimes impossible to obtain experimentally. The simulation showed surprisingly that the piece rises from the lower inner punch and dilates in the zone around the corner of the lower inner punch. In this zone, at the end of the simulation, the piece shows a defect. This type of defect exists in the

real part after ejection. The results in terms of density and force on the tools do not match perfectly with experiment results but remain within a satisfactory range.

We still have some issues we have to study further in detail: they are the constitutive relations that are appropriate for particular powders concerned, powder-wall friction that certainly vary during the compaction and elastic properties of compacts.

This paper is only concerned with the compression stage and the unloading and ejection stages have not been modeled; it is well known that many defects in the part are produced during these two stages. These points are also very important technical issues.

Finally, this study shows that the modeling need to be improved for more accurate simulations.

Acknowledgment

Part of this work was supported by 1996 Grant-in-Aid for Science and Technology (No. 96166) by the Ministry of Education, Sports and Culture.

References

1) Häggblad H.-Å., Doremus P. and Bouvard D.: "An international research program on the mechanics of powder metal forming", Advances in Powder Metall. & Particulate Materials, Vol2. Part 7, (compiled by T.M. Cadle & K.S. Narasimhan) MPIF, Princeton, (1996) 179-192.

2) J.Kergadallan, G. Puente, P. Doremus, E. Pavier: "Compression of an axisymetric part with an instrumented press", Proc. Int. Workshop on Modelling of Metal Powder Forming Processes, Grenoble, France, 1997, 277-286.

3) R.Charlier: "Approche unifiée de quelques problèmes non linéaires de mécanique des milieux continus par la méthode des éléments finis ", Ph.D. thesis, Université de LIEGE Faculté des sciences appliquées, BELGIUM, 1987.

4) P. Mosbah: "Etude expérimentale et modélisation du comportement de poudres métalliques au cours du compactage en matrice fermée", Ph.D. thesis, Université Joseph Fourier, Grenoble, 1995.

5) P. Mosbah and D. Bouvard: "Finite element simulation of die pressing compaction and ejection of iron powder", Advances in Powder Metall. & Particulate Materials, Vol2. Part 7, (compiled by T.M. Cadle & K.S. Narasimhan) MPIF, Princeton, (1996) 23-37.

6) O.C. Zienkiewicz: The finite element method, McGraw-Hill Book, 1987.

7) K.H. Roscoe and J.B.Burland: Engineering Plasticity, Cambridge Univ. Press (1968) 535.

8) E. Pavier and P. Doremus: "Mechanical behavior of a lubricated iron powder", Advances in Powder Metallurgy and Particulate Material, Vol 2, Part 6, (compiled by T.M. Cadle & K.S. Narasimhan) MPIF, Princeton, (1996), pp. 27-40.

9) P. Mosbah, D. Bouvard, E. Ouedraogo, and P.Stutz: "Experimental techniques for analysis of die pressing and ejection of metal powder, Powder Metallurgy, Vol. 40, 4 (1997) 269-277.

10) P. Doremus and E. Pavier: "Comparison between constitutive equation modelling the compaction of iron powder and experimental data obtained by triaxial tests", Proc. Int. Workshop on Modelling of Metal Powder Forming Processes, Grenoble, France, 1997, 1-8.

11) P. Mosbah, D. Bouvard, J. Lanier, E. Ouedraogo and P. Stutz: "Rheological characterization of metal powder following various loading paths", Proc. World Congress on Powder Metallurgy, Paris, 1994, Vol. 1, 677-680.
12) S. Shima and M. A. E. Saleh: "Development of Constitutive Equations for Ceramic Powders Describing Compaction-Induced Anisotropy", Mech. Materials, Vol.16, No.1-2 (1993) 73-81.
13) P. Mosbah, J. Kojima, S. Shima and H. Kotera: "Influence of third stress invariant on iron powder behavior during compaction", Proc. Int. Workshop on Modeling of Metal Powder Forming Processes, Grenoble, France, 1997, 19-28.
14) G. Coccoz, M. Bellet, R. Lecot, L. Ackerman and H. Å Häggblad: "Cold compaction of iron powder: experiments and simulations", Proc. World Congress on Powder Metallurgy, Paris, 1994, Vol. 1, 709-712.
15) M. Koerner: "Triaxial compaction of metal powder", Powder Metallurgy International, Vol. 3, No. 4, (1971) pp.86-88.
16) G.F. Bocchini: "Influence of small die width on filling and compacting densities", Powder Metallurgy, Vol. 30, No. 4, (1987) 261-266.
17) P. Mosbah, S. Shima, A.M. Habraken and R. Charlier: "Numerical simulation of multi-stepped part –A study of influence of kinematics of tooling on powder behavior-", under preparation.
18) E.Enrst and D.Barnekow: "Pressure, friction and density during axial powder compaction", Proc. World Congress on Powder Metallurgy, Paris, 1994, Vol. 1, 673-676.
19) K.J. Bathe and A. Chaudhary: "A solution method for planar and axisymmetric contact problems", Int. J. Num. Methids Eng., 21, (1985) 65-88,.
20) S. Takemoto: "The influence of powder characteristics on slip crack", Advances in Powder Metall. & Particulate Materials, Vol2. Part 7, (compiled by T.M. Cadle & K.S. Narasimhan) MPIF, Princeton, (1996) 87-100.

Table 1 Initial and final deimensions of part.

$h_{1\ initial}$	28.45 mm
$h_{2\ initial}$	54.74 mm
$h_{1\ final}$	12.63 mm
$h_{2\ final}$	26.03 mm
Initial Density	3470kg/m^3

Table 2 Tool displacement velocities in compaction stages.

Stage	1	2	3	4
Time vs. Rate displacement (Mm/s)	T=0s to T=0.39s	T=0.39s to T=0.82s	T=0.82s to T=0.96s	T=0.96s to T=1.11s
Upper punch 1	25.86	25.86	25.86	25.86
Tool 3	12.14	19.44	19.44	0
Tool 4	14.66	14.66	0	0
h_1/h_2	0.53	0.45	0.42	0.49

Table 3 Calculated and measured densities in the piece.

Zone Number	Calculated Density	Experimental Density
1	7.3	6.97
2	7.15	7.02
3	7.05	7.04
4	6.9	6.83
5	6.6	6.78

Table 4 Measured forces at end of compaction.

	Measured Forces (MN)
Upper punch	2.79
Lower inner punch	1.94
Lower outer punch	0.53

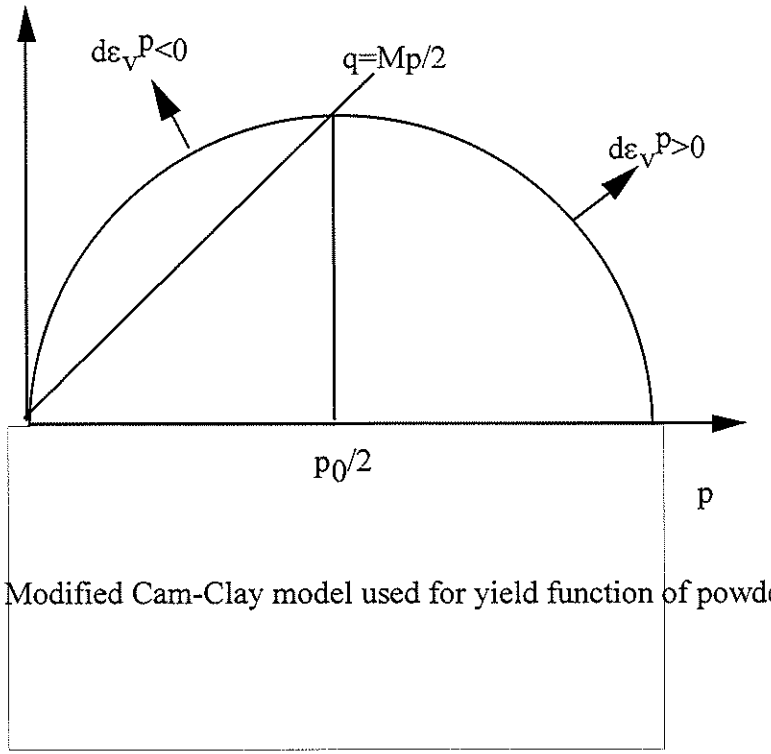

Fig.1 Modified Cam-Clay model used for yield function of powder.

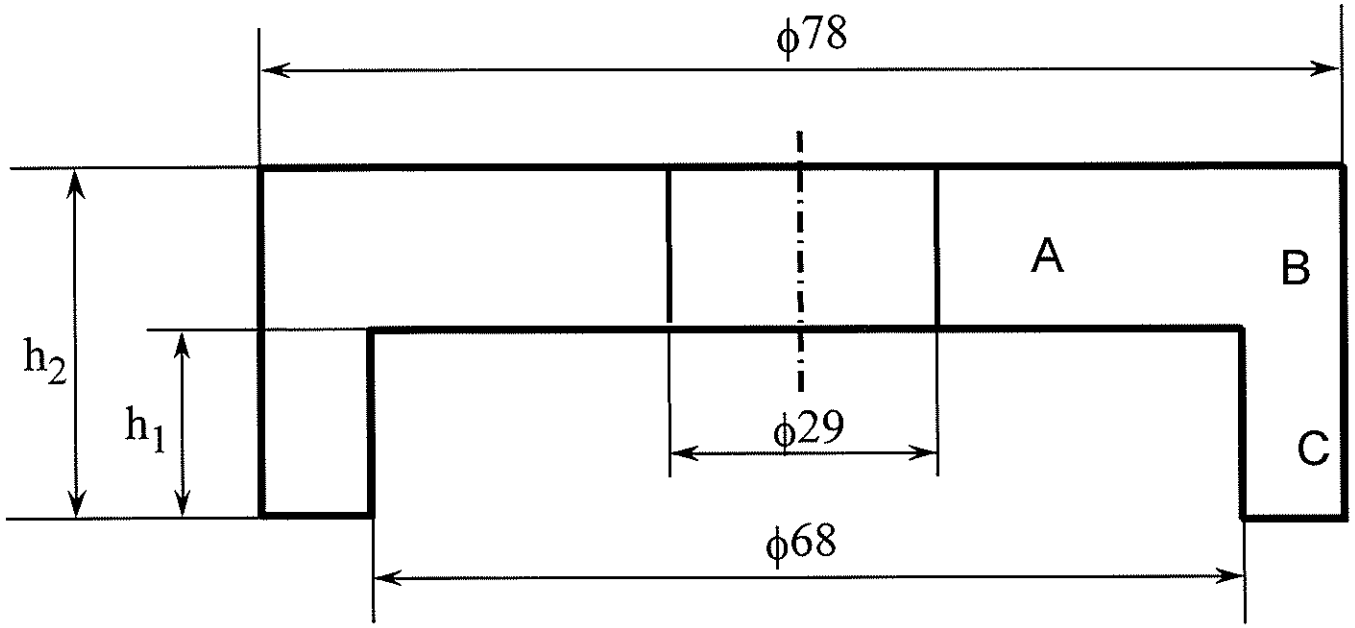

h 1initial: 28.45 mm
h_2 initial: 54.74 mm
h_1 final: 12.63 mm
h_2 final: 26.03 mm
Initial Density: 3470kg/m3

Fig.2 Shape and dimensions of final shape of compact.

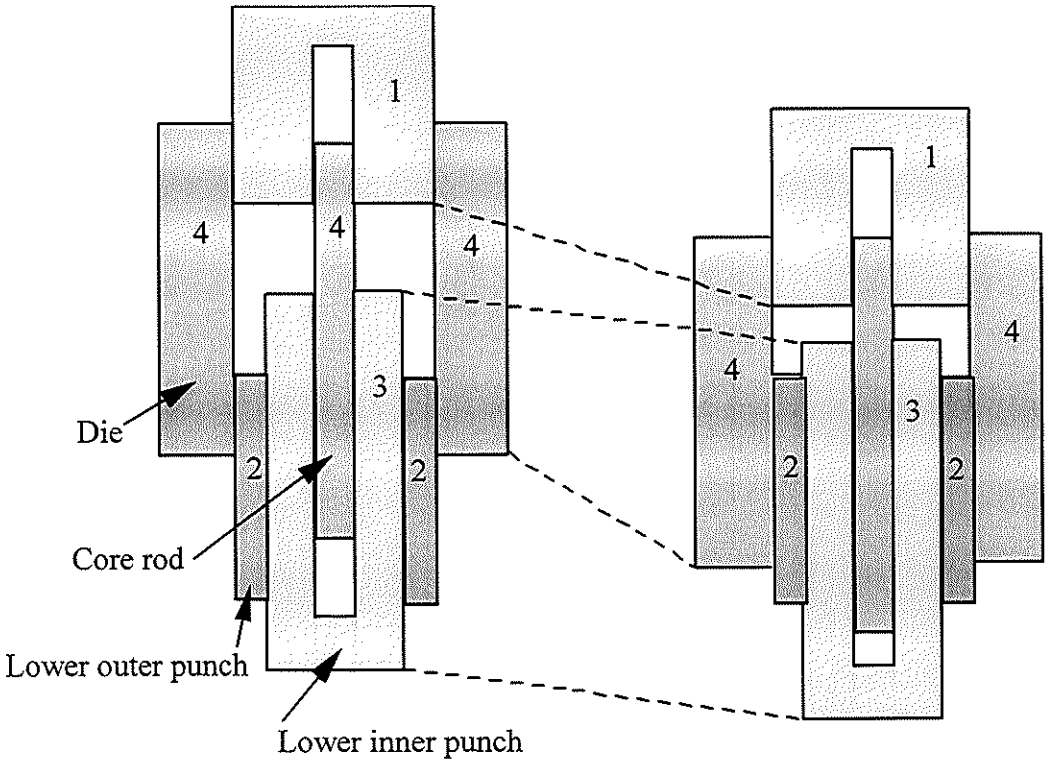

Fig.3 Initial and final positions of tools.

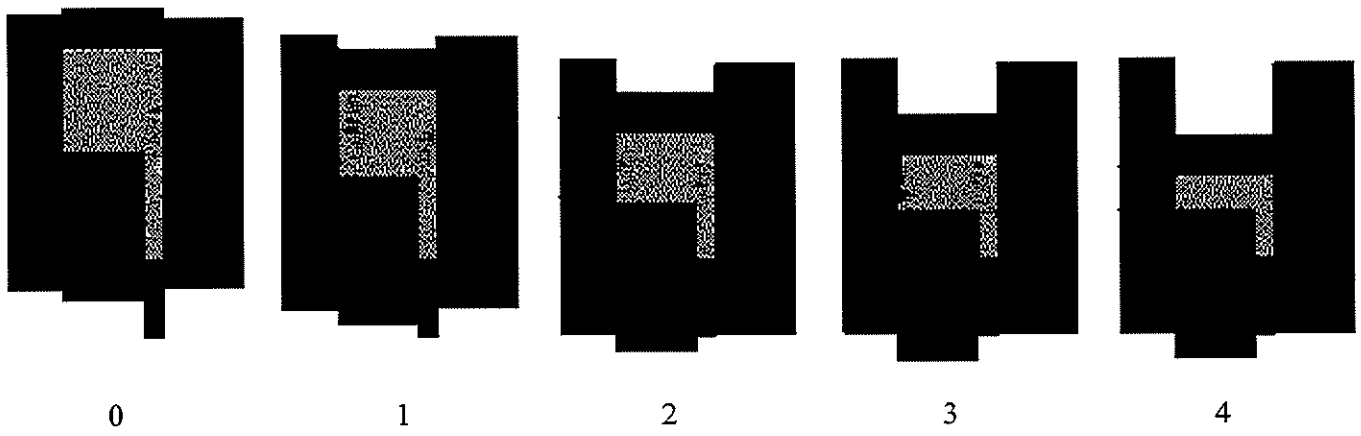

Fig.4 Kinematics of tools for compaction.

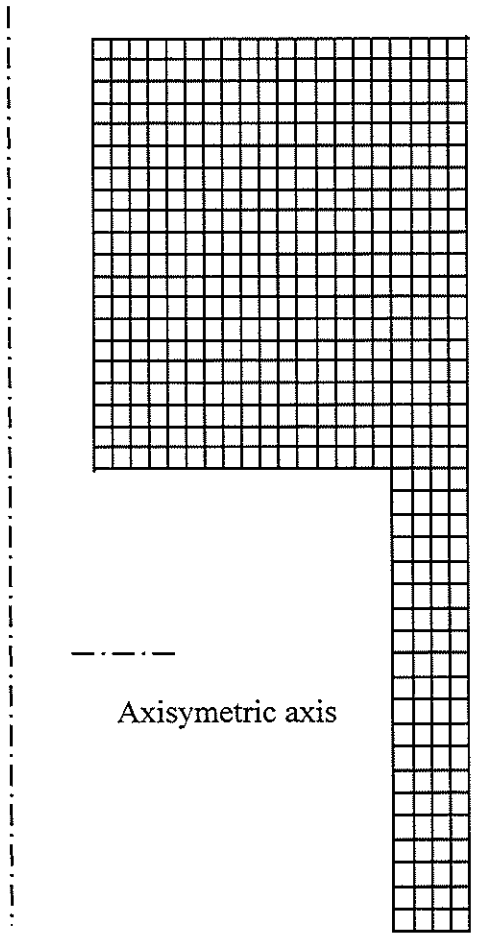

Fig.5 Finite element mesh for simulation.

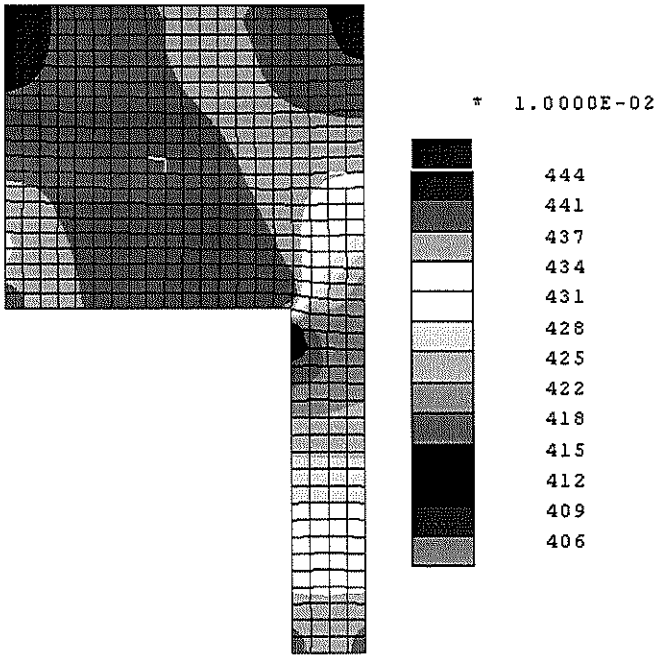

Fig.6 Density distribution at stage 1.

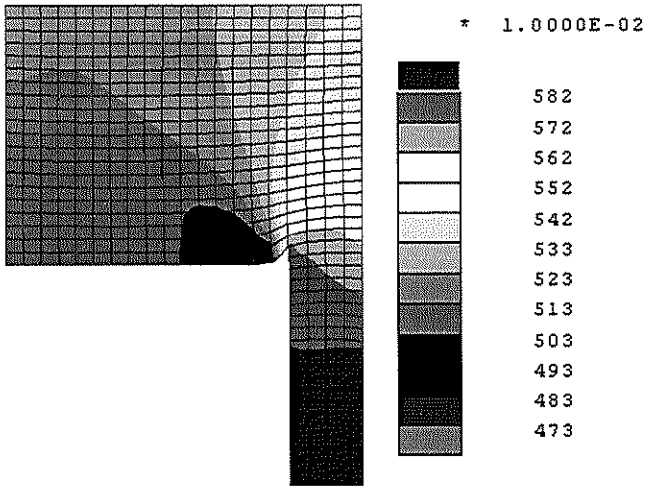

Fig.7 Density distribution at stage 2.

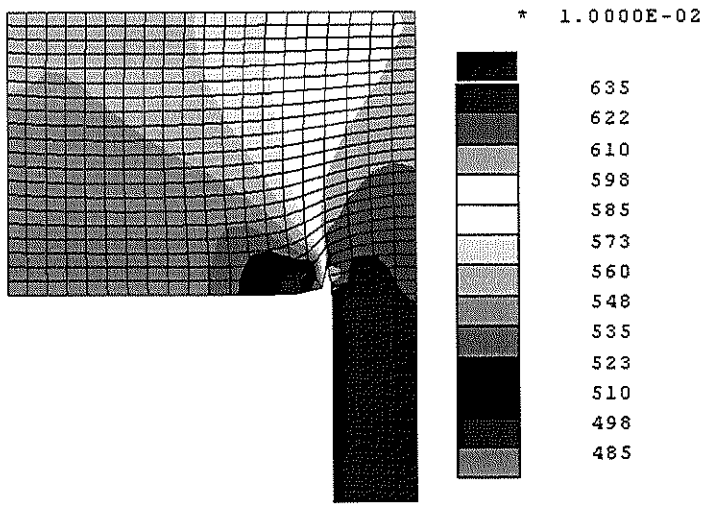

Fig.8 Density distribution at stage 3.

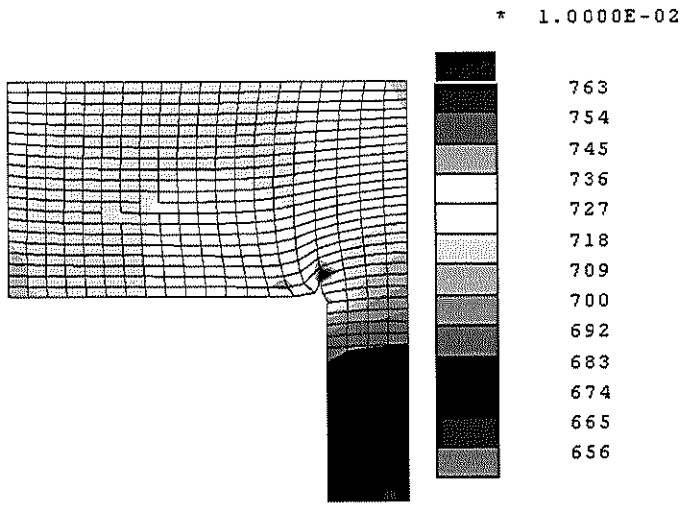

Fig.9 Density distribution at stage 4.

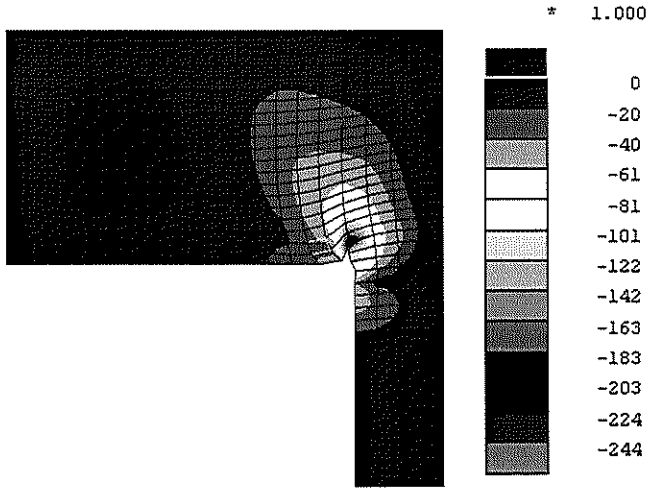

Fig.10 Shear stress distribution at final stage.

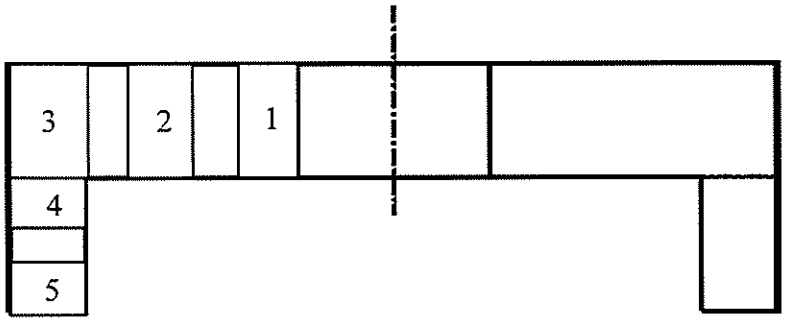

Fig.11 Zones where densiy was measured experimentally.

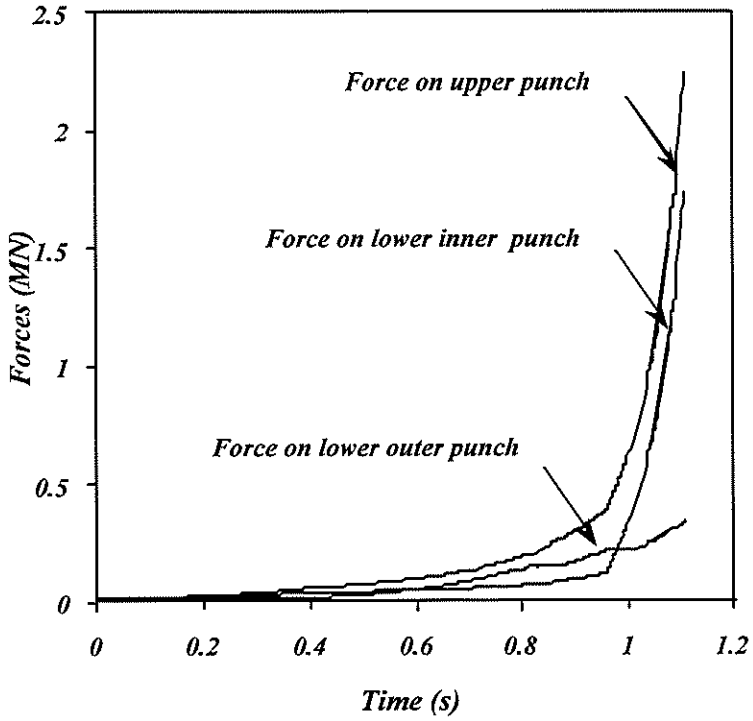

Fig.12 Calculated forces during compaction.

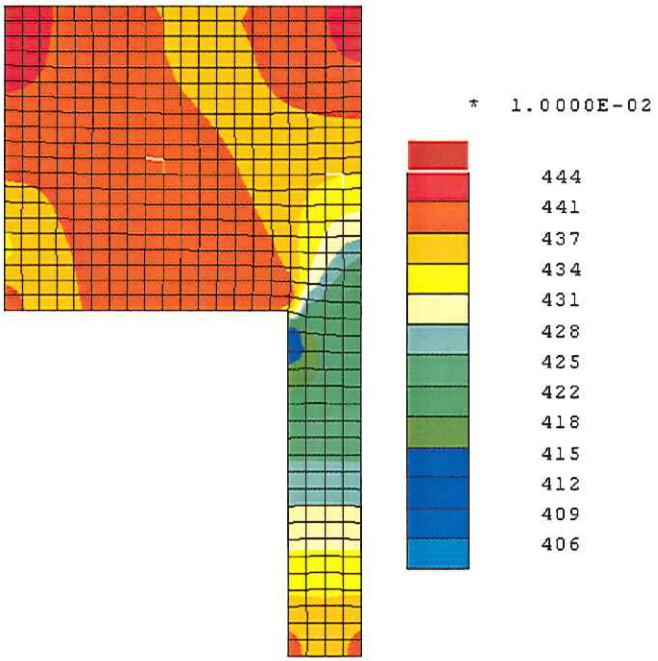

Fig.6 Density distribution at stage 1.

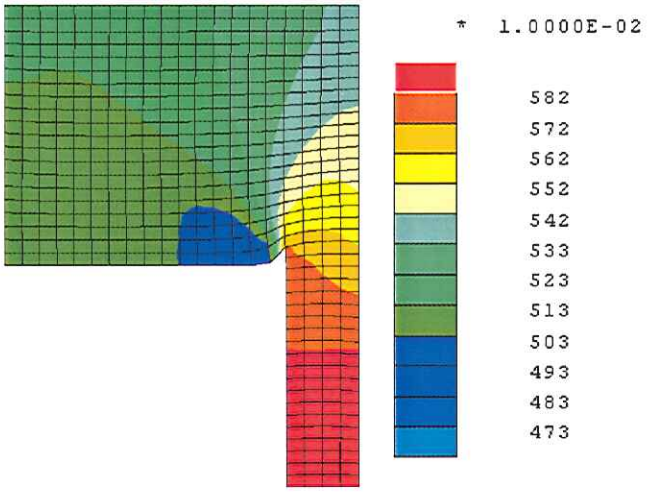

Fig.7 Density distribution at stage 2.

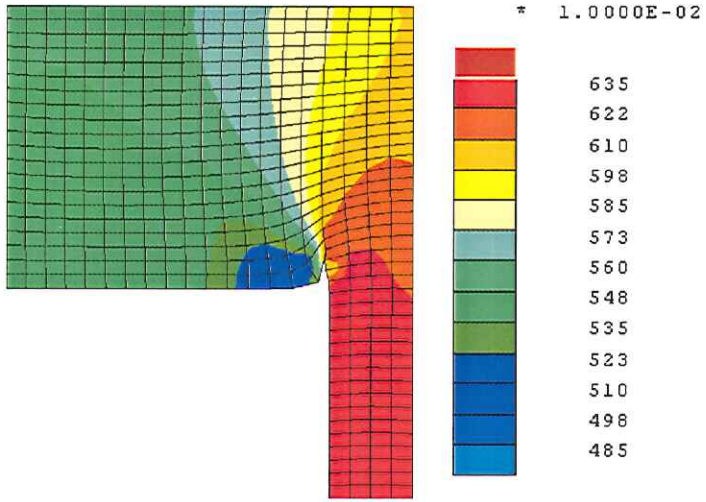

Fig.8 Density distribution at stage 3.

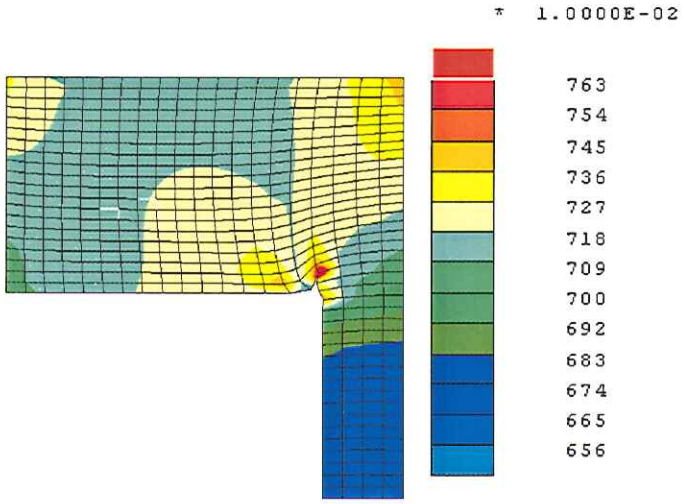

Fig 9 Density distribution at stage 4.

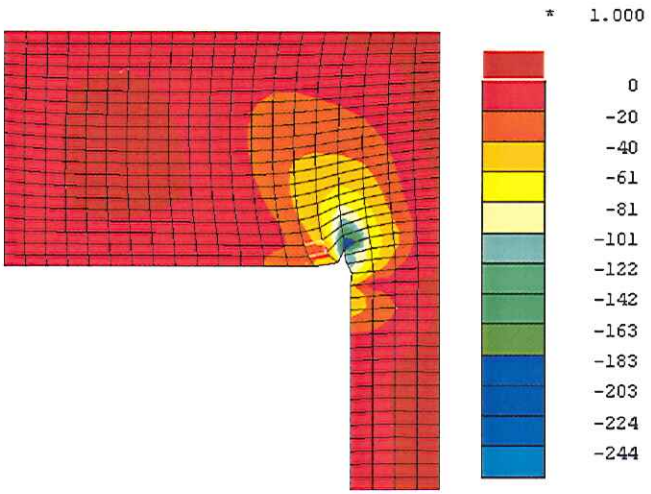

Fig.10 Shear stress distribution at final stage.